

1           **The changing character of twenty-first century precipitation over the**  
2           **western United States in the variable-resolution CESM**

3           Xingying Huang, \* Paul A. Ullrich

4           *Department of Land, Air and Water Resources, University of California, Davis*

5           \*Corresponding author address: Xingying Huang, Department of Land, Air and Water Resources,  
6           University of California Davis, Davis, CA 95616.  
7           E-mail: xyhuang@ucdavis.edu

## ABSTRACT

8 (To be added once the main content settled down)

9     **1. Introduction**

10    There is substantial and growing interest in understanding the character of precipitation within  
11    a changing climate, in large part because of the pronounced impacts of water availability on  
12    socioeconomic and natural systems (Hegerl et al. 2004; Kharin et al. 2007; Scoccimarro et al.  
13    2013). Among these studies, precipitation extremes have been a major focus, particularly drought  
14    and flood events (Seneviratne et al. 2012). Studies examining the character of precipitation in a  
15    warming world, which utilize models of varying complexity from simple thermodynamic models  
16    through complex coupled climate simulations, suggest that although atmospheric water vapor is  
17    increasing, the consequences for precipitation are far more complicated. Extreme precipitation  
18    events are particularly nuanced: Our best projections suggest that extreme precipitation events  
19    will intensify even in regions where mean precipitation decreases (Tebaldi et al. 2006; Kharin  
20    et al. 2007).

21    Although future climate projections are subject to large uncertainties, climate models are  
22    nonetheless one of the most versatile tools for studying climate variability and extremes events  
23    in the future (Easterling et al. 2000). Global climate models (GCMs) have often been used to  
24    investigate changes in the mean, variability and extremes of climate, as forced with predicted  
25    greenhouse gas (GHGs) concentrations and aerosol emissions (Meehl et al. 2006). Several past  
26    studies have investigated global impacts (Seneviratne et al. 2012), but studies addressing impacts  
27    at local and regional scales are less common. Although increased GHG concentrations have con-  
28    tributed to the observed intensification of heavy precipitation events over the tropical ocean (Allan  
29    and Soden 2008) and the majority of Northern Hemisphere overland areas Min et al. (2011), these  
30    impacts are much more poorly understood at regional scales due to variability at finer spatial scales  
31    associated with the atmospheric circulation (Trenberth 2011). As a consequence of this variability,

<sup>32</sup> a confident assessment of changes in regional extremes requires both high spatial resolution and a  
<sup>33</sup> long integration period.

<sup>34</sup> Insufficient regional-scale climate information has been a major outstanding problem in climate  
<sup>35</sup> science, as stakeholders and water managers typically require fine-scale information on climate  
<sup>36</sup> impacts in order to effectively develop adaptation and mitigation strategies. In order to reach the  
<sup>37</sup> scales needed for effective local planning, dynamical downscaling with regional climate models  
<sup>38</sup> (RCMs) has been typically used to ascertain the frequency, intensity, and duration of extreme  
<sup>39</sup> events. By only simulating a limited regional domain, RCMs better capture fine-scale dynami-  
<sup>40</sup> cal features under high horizontal resolution (Bell et al. 2004; Frei et al. 2006; Rauscher et al.  
<sup>41</sup> 2010; Wehner 2013). Higher resolution can also enable more accurate simulation of precipitation  
<sup>42</sup> extremes, which can be driven by land use, land/water contrast, snow cover, cloudiness and circu-  
<sup>43</sup> lation patterns associated with topography (Leung et al. 2003a; Diffenbaugh et al. 2005; Salathé Jr  
<sup>44</sup> et al. 2008; Wehner et al. 2010). Diffenbaugh et al. (2005) studied both heat events and wet events  
<sup>45</sup> over the contiguous United States based on RCMs simulation at 25 km horizontal resolution, and  
<sup>46</sup> demonstrated that fine-scale processes were critical for accurate assessment of local- and regional-  
<sup>47</sup> scale climate change vulnerability. Leung et al. (2003b) showed that the higher-resolution RCMs  
<sup>48</sup> yield more realistic precipitation patterns and produce more frequent heavy precipitation over the  
<sup>49</sup> western U.S. (WUS), consistent with observations.

<sup>50</sup> Despite their success, RCMs also have known issues associated with inconsistency between the  
<sup>51</sup> lateral forcing data and the driven RCM, and the menu of physical parameterizations and param-  
<sup>52</sup> eters typically available to RCMs can lead to over-tuning of the model for a particular geographic  
<sup>53</sup> region or climatological field (McDonald 2003; Laprise et al. 2008; Mesinger and Veljovic 2013).  
<sup>54</sup> Consequently, there has been growing interest in variable-resolution enabled GCMs (VRGCMs)  
<sup>55</sup> to improve regional climate simulations. Unlike RCMs, which require GCM data to drive the sim-

ulation at lateral boundaries, VRGCMs use a unified model with coarse global resolution and enhanced resolution over a specific study region (Staniforth and Mitchell 1978; Fox-Rabinovitz et al. 1997). VRGCMs have demonstrated comparable utility for regional climate studies at a reduced computational cost, particular when compared to uniform-resolution GCMs (Fox-Rabinovitz et al. 2006; Rauscher et al. 2013).

In this paper, we utilize the recently developed variable-resolution option in the Community Earth System Model (VR-CESM). VR-CESM is based on the CESM (and its predecessor, the Community Climate System Model (CCSM)), a family of models that have been used for decades to study the global climate (Neale et al. 2010a; Hurrell et al. 2013). The overall performance of VR-CESM for modeling regional climate in the California and Nevada is detailed in Huang et al. (2016), where it was argued that VR-CESM has competitive biases in comparison to the Weather Research and Forecasting (WRF) model (a traditional RCM) and the uniform-resolution CESM, when evaluating both against high-quality observations and reanalysis. VR-CESM has been used in a number of studies to capture fine-scale atmospheric processes (Zarzycki et al. 2014, 2015; Rhoades et al. 2015). It was also shown that VR-CESM did not suffer from apparent artifacts within the coarse-fine transition region.

This study focuses on changes in the character of precipitation over the 21st Century within the WUS, as predicted from long-term ensemble runs conducted with VR-CESM with a local grid resolution of  $\sim 0.25^\circ$ . The WUS is known to be particularly vulnerable to hydrological extreme events, particularly floods and droughts (Leung et al. 2003b; Caldwell 2010), and hosts a variety of local features and microclimates associated with its rough and varied topography. Simulations of the future climate are performed in accordance with the representative concentration pathway (RCP) 8.5 scenario, which describes a “business-as-usual” projection for GHGs (Riahi et al. 2011). RCP8.5 is a baseline scenario with updated base year calibration (to 2005) and no

80 explicit climate policy. In this study we focus on a single RCP since end-of-century projections  
81 with the substantially more optimistic RCP2.6 scenario have been found to be qualitatively sim-  
82 ilar to mid-century RCP8.5 results (which are assessed in this study). Simulations are further  
83 conducted in accordance with the Atmospheric Model Intercomparison Project (AMIP) protocol  
84 (Gates 1992), a widely-used approach for climate model diagnosis, validation and intercompari-  
85 son that imposes global sea surface temperatures (SSTs) and sea ice. By constraining atmospheric  
86 boundary conditions at the sea surface, we avoid model biases that are known to exist in the fully  
87 coupled configuration (Grodsky et al. 2012; Small et al. 2014) and accept potential uncertainties  
88 associated with our choice of SSTs.

89 Changes in the character of precipitation, in terms of frequency and intensity, have been assessed  
90 in our study from recent history through the end of 21st century. A comprehensive set of metrics  
91 for precipitation extremes have been evaluated from ensemble simulations over the 26-year peri-  
92 ods corresponding to historical (1980-2005), mid-century (2025-2050) and end-of-century (2075-  
93 2100). We hypothesize that spatial inhomogeneity in local geography and temperature will also  
94 result in similarly inhomogeneous impacts on the precipitation field. We expect that teleconnec-  
95 tions (specifically the El Niño-Southern Oscillation, ENSO) will have a pronounced impact on  
96 precipitation features over particular area under the changes of mean SST and its variations. Since  
97 only one SST dataset was used for this study, we note that our projections are conditioned on a  
98 particular future character of ENSO. This is a potentially large source of uncertainty, as at present  
99 there is no clear consensus on how ENSO may behave under a warming climate (Fedorov and  
100 Philander 2000; Guilyardi et al. 2009), and strengthening or weakening of this pattern will have  
101 clear consequences for our results.

102 This work builds on a number of previous studies that have explored the projected future change  
103 in WUS precipitation. For example, Kim (2005) applied downscaled climate change signals to se-

104 lected indicators, and concluded that global warming induced by increased CO<sub>2</sub> is likely to drive  
105 increases in extreme hydrologic events in the WUS. Duffy et al. (2006) found that mean precip-  
106 itation predicted by the RCMs are not statistically significant compared to interannual variability  
107 in many regions over WUS, although there is little consistency among the different RCMs as to  
108 responses in precipitation to increased GHGs. Gao et al. (2015) pointed out a potentially large  
109 increase in atmospheric river events by the end of the 21st century under the RCP8.5 scenario.

110 This paper is structured as follows. Section 2 describes the model setup. Section 3 describes  
111 the methodology and reference datasets employed. An assessment of the ability of the model to  
112 capture the climatology of the WUS is given in section 4. Results from the future mean climato-  
113 logical trend and projected changes to precipitation indices are in section 6. Section 7 summarizes  
114 the main points of the study along with further discussion.

## 115 2. Model Setup

116 CESM is a state-of-the-art Earth modeling framework, consisting of coupled atmosphere, ocean,  
117 land and sea ice models (Neale et al. 2010b; Hurrell et al. 2013). In this study, the Community At-  
118 mosphere Model version 5 (CAM5) (Neale et al. 2010b) and the Community Land Model version  
119 4.0 (Oleson et al. 2010) are used. CAM5 is configured with the Spectral Element (SE) dynamical  
120 core, which supports desirable conservation, accuracy and parallel scalability properties (Dennis  
121 et al. 2011; Taylor 2011) and incorporates the variable-resolution option (Zarzycki et al. 2014).  
122 CLM is employed in the *unigrid* configuration, which allows the land model and atmospheric  
123 model to utilize the same model grid so eliminates the need for interpolation. SSTs and sea ice,  
124 which are used to compute ocean-atmosphere fluxes, are prescribed in accordance with the AMIP  
125 protocol (Gates 1992). The variable-resolution mesh used for this study is depicted in Figure 1, in  
126 accord with our past studies (Rhoades et al. 2015; Huang et al. 2016; Huang and Ullrich 2016).

127 Simulations have been performed for the historical period (1979-2005, hereafter referred to as  
128 `hist`) and for two future periods: 2024-2050 (hereafter referred to as `mid`) and 2074-2100 (hereafter  
129 referred to as `end`). Daily output are recorded for each period on the native SE grid and then  
130 remapped to a regional latitude-longitude mesh (??). For purposes of analysis, the first year of  
131 each time period was discarded as a spin-up period to allow adequate time for the initialized land  
132 and atmosphere to equilibrate. The 26-year duration was chosen to provide an adequate sampling  
133 of annual variability for each time phase. As mentioned earlier, GHG concentrations are set based  
134 on RCP8.5. Historical SSTs and sea ice are prescribed at 1° resolution, as described by Hurrell  
135 et al. (2008). SSTs and sea ice for each future period are developed from fully-coupled RCP 8.5  
136 climate simulations with bias correction applied (Cecile Hannay, personal communication). Using  
137 prescribed SSTs in place of a coupled ocean model considerably reduces the computation cost and  
138 so allows the atmospheric model to be run at a higher overall resolution. Annually-updated land  
139 surface datasets, which prescribe land-use characteristics, are interpolated from 0.5° to the land  
140 model grid.

141 Ensemble runs are needed to ensure that the sample adequately accounts for climate variability,  
142 especially for statistics associated with climatological extremes. However, the exact number of  
143 ensemble members required is heavily dependent on the variability of the particular metric being  
144 examined, and so no standard ensemble criteria exists. Deser et al. (2012b) suggest that around  
145 3 ensemble runs are required to detect a significant epoch difference for JJA (June-July-August)  
146 surface temperatures, whereas 10 to 30 ensemble members are needed for that for DJF (Dec.-Jan.-  
147 Feb.) precipitation. In our study, the use of prescribed SSTs does reduce the intrinsic variability  
148 of the climate system (see supplement), and so we found reasonably converged results with two  
149 ensemble members for the historical period and four ensemble members for each future period.

150 **3. Methodology**

151 *a. Precipitation indices*

152 Standard indices have been employed to characterize precipitation (Tebaldi et al. 2006; Zhang  
153 et al. 2011; Sillmann et al. 2013). In order to choose a comprehensive (but minimal) set that are  
154 informative to stakeholders and water managers, indices from throughout the literature have been  
155 assessed. The indices examined include those defined by the Expert Team on Climate Change De-  
156 tection and Indices (ETCCDI) (Karl et al. 1999) that are featured in earlier studies (Dulière et al.  
157 2011; Sillmann et al. 2013; Diffenbaugh et al. 2005; Singh et al. 2013) and others such as return  
158 levels, dry spell and wet spell characteristics defined by either percentiles or by selected thresh-  
159 olds. The indices we have chosen for this study attempt to provide a relatively comprehensive  
160 characterization of precipitation, and are summarized in Table 1.

161 [Paul: You should probably state at some point why you don't employ drought or dry spell  
162 indices]

163 *b. Impacts of ENSO*

164 The impact of ENSO on precipitation is emphasized in our study due to its influence on precipi-  
165 tation over a majority of our study area, particularly the southwest U.S. (Cayan et al. 1999; Zhang  
166 et al. 2010; Deser et al. 2012a; Yoon et al. 2015). The phase of ENSO (*i.e.* El Niño and La Niña)  
167 is identified each year using the Oceanic Niño Index (ONI), defined as the 3-month running means  
168 of SST anomalies in the Niño 3.4 region (covering 5N-5S, 120-170W based on NOAA (2013)).  
169 An El Niño or La Niña episode is said to occur when the ONI exceeds +0.5 or -0.5 for at least five  
170 consecutive months for a water year (*i.e.* from July to June) (NOAA 2013) (see the supplement).  
171 In order to adjust for the trend in the SST field associated with climate change, the anomaly is

172 computed against the detrended mean SSTs from the periods 1971-2000, 2020-2050 and 2070-  
173 2100 for hist, mid and end respectively, using the aforementioned observed and predicted SST  
174 datasets. As argued by Kao and Yu (2009), it may be desirable to use an extended Niño 3.4 region  
175 to determine the phase of ENSO – however, when employing SST anomalies integrated over the  
176 region 105-170W, we observed no significant impact on ONI statistics.

177 *c. Assessing statistical significance*

178 Student's t-test has been used to test whether or not two datasets at each grid point are statisti-  
179 cally equivalent, if the sample population can be adequately described by a normal distribution.  
180 The normality of a dataset is assessed under the Anderson-Darling test. When the sample popu-  
181 lations do not approximately follow a normal distribution, Mann-Whitney-Wilcoxon (MWW) test  
182 is employed in lieu of the t-test. All these tests are evaluated at the 0.05 ( $\alpha$ ) significance level.  
183 When comparing different time periods, statistical tests are conducted using all years from each  
184 ensemble run.

185 (add description of the supplement like what are included; see the sst\_enso.pdf, mask the land  
186 (over land, it should the surface temperature.))

187 *d. Reference datasets*

188 Gridded observational datasets and reanalysis of the highest available quality, with comparable  
189 horizontal resolutions to our VR-CESM simulations, are used for assessing the simulation qual-  
190 ity. Multiple reference datasets are necessary due to the underlying uncertainty in interpolating  
191 precipitation fields. The three datasets employed are as follows:

192 **UW Gridded Data:** The  $0.125^\circ$  UW daily gridded meteorological data is obtained from  
193 the Surface Water Modeling group at the University of Washington, covering the period

194 1949-2010 (Maurer et al. 2002; Hamlet and Lettenmaier 2005). The UW dataset imposes  
195 topographic corrections by forcing the long-term average precipitation to match that of the  
196 PRISM dataset.

197 **National Centers for Environmental Prediction (NCEP) Climate Prediction Center**  
198 **(CPC):** This  $0.25^{\circ}$  daily-output dataset provides gauge-based analysis of daily precipitation  
199 from the CPC covering the period 1948-2006. It is a unified precipitation product that cov-  
200 ers the Conterminous United States and amalgamates a number of data sources at CPC via  
201 optimal interpolation objective analysis.

202 **North American Regional Reanalysis (NARR):** NARR is a  $\sim 32$  km high-resolution reanal-  
203 ysis product with 3-hourly output produced by NCEP via dynamical downscaling over North  
204 America and covering the period 1979-present (Mesinger et al. 2006).

## 205 **4. Model Assessment**

206 Before proceeding, we assess the ability of VR-CESM to represent the character of precipitation  
207 over the WUS. The indices defined in Table 1 are depicted in Figures 2 and Figure 3 for VR-  
208 CESM and each of the reference datasets over the historical period (1980-2005). We assume  
209 equal confidence in each of the reference datasets, and use Student's t-test (with UW, CPC and  
210 NARR as the three statistical samples) to identify regions where VR-CESM deviates significantly  
211 from the reference mean. Regions where differences are statistically significant are identified with  
212 stippling in row (a) and (e) of each figure.

213 Compared against the reference, VR-CESM largely captures the spatial patterns of precipitation  
214 and its indices. As expected, the majority of precipitation distributed along the northwest coastal

215 area and the mountainous regions of the Cascades and the Sierra Nevada. Nonetheless, several  
216 apparent biases are present:

217 First, VR-CESM significantly overestimates Pr over dry regions with deviations between 0.2 mm  
218 to 1.5 mm, especially over the eastern flank of the Cascades and on both sides of the Sierra Nevada  
219 (with relative differences reaching 50%-150%). As with many regional models, VR-CESM is  
220 “dreary” and exhibits too many precipitation days ( $R1mm$ ,  $Pr \geq 1$  mm/day and  $R5mm$ , 1 mm/day  $\leq$   
221  $Pr \leq 5$  mm/day) [citation needed]. Nonetheless, over most regions the relative contribution of each  
222 precipitation frequency subset to total precipitation ( $F1mm$ ,  $F5mm$ ,  $F10mm$ ,  $F20mm$ ,  $F40mm$ ) is  
223 fairly accurate, suggesting that the probability density function describing precipitation intensity  
224 is accurately represented almost everywhere.

225 Second, the spatial pattern of precipitation variability agrees well between VR-CESM and ref-  
226 erences with agreement everywhere except in the Great Plains (the eastern edge of our domain)  
227 and in California’s Central Valley. The Great Plains is not a focus of this study, but the suppressed  
228 variance is dominant during the warm season (April-September) and so likely represents a failure  
229 of the convection scheme to adequately simulate variability in this region. This bias is also ob-  
230 served in  $0.25^\circ$  uniform-resolution CESM simulations [citation needed to ASD data], and so is not  
231 a symptom of the eastern edge of the variable-resolution transition region.

232 However, the grossly exaggerated variability over the western flank of the Sierra Nevada through  
233 California’s Central Valley does merit some additional discussion. Here, the overestimation of  
234 precipitation and enhanced variability is associated with too many extreme precipitation events  
235 ( $Pr > 20$  mm/day). This bias is related to exaggerated orographic uplift (upslope winds, not shown)  
236 and is associated with a dry bias along the eastern flank of the Sierras. Similar biases in simulating  
237 extreme precipitation over the topographically complex regions including the Cascades and Sierra  
238 Nevada ranges have also been found in high-resolution RCM simulations Walker and Diffenbaugh

239 (2009); Singh et al. (2013), and have been primarily attributed to excessively strong winds. This  
240 issue may be further impacted by the diagnostic treatment of precipitation in CAM5 [citation to  
241 Morrison Gettleman 1 microphysics].

242 The representation of precipitation in VR-CESM over California was also discussed in Huang  
243 et al. (2016), where it was observed that VR-CESM simulations at  $0.25^\circ$  adequately represented  
244 regional climatological patterns with high spatial correlation. VR-CESM demonstrated compa-  
245 rable performance to WRF at 27 km (which was forced with ERA-Interim reanalysis), but still  
246 overestimated overall winter precipitation (by about 25%-35%) compared to reference datasets,  
247 with the largest differences over the western edge of the Sierra Nevada. This bias is not allevi-  
248 ated by simply increasing the spatial resolution, as experimental VR-CESM simulations at 14km,  
249 7km and 3.5km show only modest improvement (Alan M. Rhoades, personal communication).  
250 This suggests that the bias might be related with more complex dynamic processes rather than  
251 treatment of the orographic effects.

252 CESM at 1 degree resolution was also assessed in order to better understand the impacts of res-  
253 olution. We find that precipitation patterns over complex topography are poorly represented and  
254 do not capture the spatial patterns induced by orographic effects. Over the Cascades and Sierra  
255 Nevada, total precipitation grossly underestimated by  $1^\circ$  CESM, when compared to VR-CESM,  
256 gridded and reanalysis datasets (see the supplement [Point to exact figure]). Precipitation has oth-  
257 erwise been smoothed out over the coastal areas and the mountainous regions of the northwest U.S  
258 when simulated with CESM at coarse resolution. This result clearly underscores the benefits of  
259 high resolution (particularly the representation of topography) in simulating precipitation features.  
260 Results are also provided in the supplement for the output from a globally-uniform CESM run at  
261  $0.25^\circ$  spatial resolution with the finite volume (FV) dynamical core (Wehner et al. 2014), which  
262 exhibits similar performance to VR-CESM (see the supplement [Point to exact figure]). Overall,

263 0.25° resolution appears to provide the best tradeoff between accuracy and computational cost, as  
264 coarser resolution does not correctly represent precipitation features and higher resolution does  
265 not appear to substantially improve model accuracy.

266 We have also assessed the impact of the ENSO signal within the historical VR-CESM runs by  
267 differencing the precipitation fields between the warm phase (i.e. El Niño) and cool phase (i.e.  
268 La Niña), compared to references (see the supplement). ENSO exhibits a weaker signal for obser-  
269 vational precipitation, compared to VR-CESM, which might suggest that the model exaggerates  
270 ENSO's impact on precipitation, especially over the northwest U.S. The improvement of ENSO  
271 in the model is directly proportional to the representation of ENSO forced precipitation anomalies  
272 (AchutaRao and Sperber 2006).

## 273 5. Drivers of climatological precipitation

274 Precipitation has been observed and modeled to being changed both regionally and globally  
275 under climate warming as discussed in the introduction. The observed intensification of heavy  
276 precipitation events over the the latter half of the twentieth century is attributed to the human-  
277 induced increases in GHGs over majority of Northern Hemisphere land areas (Min et al. 2011),  
278 although no significant changes in the total precipitation has been observed globally (Donat et al.  
279 2016). With the coupled effects of continued increasing CO<sub>2</sub> and SSTs in the future, precipitation  
280 is assumed to be changed driven by both the radiative changes in the lower troposphere and inten-  
281 sified water vapor evaporation over the ocean (Allen and Ingram 2002; Sugi and Yoshimura 2004).

282 Precipitation extremes are projected to intensify continuously through the end of 21st century in  
283 both dry and wet regions with heterogeneous patterns (Donat et al. 2016).

284 As described by the Clausius-Clapeyron (C-C) equation, the water vapor content is supposed  
285 to increase by ~7% for each 1°C increase in temperature (Allan and Soden 2008). Naturally,

286 evaporation over the ocean will increase with the climate warming, but the increasing rate may be  
287 constrained over land due to limitations by soil moisture (Cayan et al. 2010). When the air holds  
288 more water vapor, the chances of heavy rain events tend to increase even at which total precipita-  
289 tion is decreasing (Trenberth 2011), given that global total precipitation is expected to increase at  
290 a lower rate than precipitation extremes (Allan and Soden 2008). According to previous studies  
291 (e.g. (Allan and Soden 2008; O’Gorman and Schneider 2009; Min et al. 2011)), changes in more  
292 extreme precipitation follow the C-C relationship more closely than total precipitation amount  
293 (Trenberth et al. 2003). However, those changes are still remain uncertain with the increasing rate  
294 of precipitation extremes affected by multiple factors including the vertical velocity profile and  
295 temperature changes (O’Gorman and Schneider 2009).

296 The moderate or heavy precipitation events over WUS mainly result from the large-scale water  
297 flux transport from the eastern Pacific Ocean rather than directly from evaporation, usually in  
298 the form of atmospheric rivers (ARs) or orographic updraft (Trenberth et al. 2003; Neiman et al.  
299 2008). The storm track may be enhanced, which would increase ARs along the U.S. west coast  
300 with increased air water vapor content in the future (Dettinger 2011; Gao et al. 2015). In the  
301 following section, both the mean changes of precipitation and distributions of both non-extreme  
302 and extreme events are investigated as projected by the VR-CESM model under an extreme climate  
303 forcing context(i.e. RCP 8.5).

304 The precipitation of WUS has strong inter-annual variability caused by large-scale atmospheric  
305 circulation mainly associated with the ENSO (Leung et al. 2003b). As a significant driver  
306 of precipitation, ENSO modulates the storm track behavior over western U.S. with a north-  
307 west/southwest precipitation dipole (Gershunov and Barnett 1998), as discussed in 2. The pro-  
308 jected SSTs we used here states one of the possible cases of ENSO scenarios in the future. How-  
309 ever, there is still substantial uncertainty regarding how El Niño will change under global warming

310 (Fedorov and Philander 2000; Guilyardi et al. 2009), resulting corresponding uncertainty in our  
311 results. Capotondi (2013) showed that the diversity of El Niño characteristics in CCSM4 is com-  
312 parable to what was found in observations, although, as found by Deser et al. (2012c), the overall  
313 magnitude of ENSO in CCSM4 is overestimated by 30% over the preindustrial time period.

## 314 6. Results

### 315 a. Mean climatology

316 Before proceeding with the analysis of precipitation features, it is first important to understand  
317 how the mean climatology changes in VR-CESM across time periods (Figure 4). Since the charac-  
318 ter of WUS precipitation has a strong seasonal dependence, the mean climatology including mean  
319 precipitation, near-surface temperature and near-surface relative humidity are depicted in two sea-  
320 sons including the cool season (or wet season) from October to March and the warm season (or  
321 dry season) from April to September.

322 As a result of enhanced GHG concentrations, mean annual near-surface temperature (T2avg)  
323 increases by about 1.5 to 2 K from hist to mid and about 4 to 6 K from mid to end. Despite the  
324 large spatial variation in climatological temperatures, the temperature change between historical  
325 and future is fairly uniform. However, there is a slightly weaker increase in the near-coastal  
326 regions during cool season and in the lower latitude area at warm season, which might be due to  
327 the increased westerly wind during cool seasons and northward wind during warm season from  
328 the near ocean. Larger increases of temperature is also observed in warm season than cool season  
329 for about 0.5 K and 1 K for mid and end respectively.

330 Practically, whether the increase rate of the water vapor as the temperature goes up will keep the  
331 same or not will directly affect the relative humidity. As water vapor reaches saturation, conden-

332 sation triggers clouds and precipitation. To understand the increasing rate of water vapor content  
333 under climate warming and whether relative humidity can be remain or not, 2m relative humidity  
334 (RH) is plotted in Figure 4.

335 Overall, RH remains almost the same as `hist` over the regions where temperature does not sub-  
336 stantially increase. However, in regions where temperature increase is larger than 2 K, RH is  
337 instead observed to decrease significantly relative to historical values for about 2% and 3-6%  
338 compared to `mid` and `end` respectively. In fact, trends in RH are spatially consistent with tempera-  
339 ture increase but opposite in magnitude with a spatial correlation coefficient of approximately 0.8.  
340 RH still remains the same or increase over part of the near-coastal area over the Pacific Ocean due  
341 to the lower increase of T2avg compared to the land area. This suggests that continental evapo-  
342 ration and oceanic water vapor transport are insufficient to compensate for the air vapor capacity  
343 when temperature increases to certain level, which is consistent with Joshi et al. (2008), and has  
344 been observed in results by Rowell and Jones (2006) over continental and southeastern Europe  
345 and Simmons et al. (2010) over low-latitude and midlatitude land areas.

346 Based on those background changes of heat and water vapor, from `hist` to `mid`, mean precipita-  
347 tion showed a 0.2-0.6 mm/day increase during cool season with a largest change over northwest  
348 and less than 0.2 mm/day during warm season over southeast part. From `hist` to `end`, the increase is  
349 about 0.4-1.2 mm/day during cool season with also a largest change over northwest, and no notable  
350 change is observed during warm season. Nonetheless, these results are statistically significant (see  
351 Figure 5). East of the Rockies, precipitation increases through mid-century (statistically signifi-  
352 cant), but this trend appears to recede towards the end of the century (although these results are not  
353 significant). There is also a decrease of about 0.1mm/day in total precipitation over the western  
354 flank of the Sierra Nevadas during the cool season from `hist` to future. This decrease (about 0.15  
355 mm/day) is also found over the Cascades and the western coastal area during warm season from

hist to mid. However, this decrease is not statistically significant. Majority of the precipitation over the cool season emerged from large-scale patterns, whereas warm season precipitation was from convection processes. The precipitation over WUS for moderate or heavy precipitation is mainly due to the large-scale water flux transport from the eastern Pacific Ocean rather than directly from evaporation, mainly in the form of atmospheric rivers or orographic updraft (Trenberth et al. 2003; Neiman et al. 2008).

The increase of mean wet season precipitation over the northwest is mainly caused by the enhanced orographic precipitation due to increased integrated vapor transport (IVT). The IVT increases due to higher water vapor content from increased ocean evaporation, which is affected primarily by climatological forcing. Over southern California, precipitation did not show significant changes since no substantial increase in IVT over Eastern Pacific Ocean near southern California coast is predicted, with IVT in this region driven primarily by variations in ENSO. Since precipitation over the Intermountain West during warm season is mainly results from the convection processes, precipitation is directly related with the changes of the relative humidity. As shown in Figure 4, RH has decreased over most the study area except over where the soil moisture is relatively low when going to end. Further, the changes of RH are related with the soil moisture magnitude accompanying the changes of latent heat flux during warm season.

According to previous studies (e.g. (Allen and Ingram 2002; Allan and Soden 2008; O’Gorman and Schneider 2009; Min et al. 2011)), changes in more extreme precipitation follow the C-C relationship more closely than total precipitation amount (Trenberth et al. 2003). In order to find out the precipitation changes in a comprehensive aspect based on our fine-scale simulations, analyses of different precipitation distributions are focused in the following part to account for the future changes of diverse precipitation events.

379    *b. Precipitation indices*

380    To see how precipitation changes in a comprehensive way, we have analyzed detailed precipita-  
381    tion distributions in order to account for the future changes of different precipitation events, based  
382    on our simulation results. The precipitation indices are presented in Table 1. For each index, the  
383    changes of precipitation character for each period, averaged over all ensemble members are plotted  
384    in Figure 5 (for the indices that quantify precipitation days) and Figure 6 (for the indices describing  
385    precipitation amounts). Although mean precipitation shows a weak but overall increasing trend  
386    from hist to mid and mid to end (about 10-15%), the precipitation indices exhibit substantially  
387    more unique character.

388    When comparing hist to mid, the total rainy days and frequency of non-extreme precipitation  
389    have significantly increased (about 10-15%) mainly over the central-east and southeast part of  
390    WUS, which is less obvious between mid and end. On the contrary, the frequency of non-extreme  
391    precipitation have decreased significantly over the northwest region and the eastern part of the  
392    Montana, Wyoming and Oregon from mid to end (about 10%). These changes are the primary  
393    driver for the observed change to mean precipitation exhibited in Figure 4.

394    As for extreme precipitation frequency (i.e. days with daily Pr between 10 mm and 40 mm), the  
395    number of days increases from hist to mid, but the pattern is scattered over northwest and central  
396    WUS. When comparing mid to end, there is a clear and significant increase in extreme precip-  
397    itation events over the northwest coastal area (about 20-30%) and eastern flank of the Cascades  
398    (larger than 40%). This result is consistent with Dominguez et al. (2012), who observe a robust  
399    increase in winter precipitation extremes toward the latter half of the 21st century by an ensemble  
400    of RCMs. There is a slight, but insignificant decrease over the Cascades and the Sierra Nevada

401 (significance is low due to the high variability of precipitation). No notable predicted changes have  
402 been observed over California.

403 The associated precipitation signal under a warmer climate is more ambiguous for California  
404 (Neelin et al. 2013) considering the extreme variability on interannual time scales (Dettinger  
405 2011). Kim (2005) found that under global warming, heavy precipitation events show largest  
406 increases in the mountainous regions of the northern California Coastal Range and the Sierra  
407 Nevada. However, our results show a minor decrease (though not statistically significant) of ex-  
408 treme precipitation over the Sierra Nevada. The decrease over southwest U.S. is mainly due to the  
409 intensified La Niña in the future as shown in the Section 2.

410 For very extreme precipitation ( $\text{Pr} \geq 40 \text{ mm}$ ) events, there is an increasing trend over the north-  
411 west coast (larger than 60%) and the Cascades (about 50%) and its eastern flank (larger than 60%)  
412 when comparing `hist` to `end`. Significant changes have also observed over the northern moun-  
413 tainous part of California for about 20-40% from `hist` to `end`. The corresponding changes in rain  
414 amount are consistent with the changes of frequency (see Figure 6). Overall, these results indi-  
415 cate more extreme precipitation over the northwest U.S with changes in precipitation extremes  
416 following more consistently with the C-C relationship.

417 In order to understand the drivers behind the observed changes, we first examine change in  
418 moisture flux for cool seasons when WUS precipitation is primarily from water vapor influx from  
419 the Pacific Ocean (see Figure 7). We observe an increase in specific humidity at 850 hPa that  
420 accompanies the increase of the temperature in future. **However, when comparing to `hist`, westerly**  
421 **wind tends to weaken in mid and end over the eastern part of the WUS and strengthen over western**  
422 **area.**

423 IVT (Figure 7) for extreme precipitation days over cool seasons. Generally, IVT is useful to  
424 understand extreme precipitation events that arise from atmospheric rivers over the northwestern

425 U.S. and from orographic uplift (especially for very extreme precipitation) (Ralph et al. 2004;  
426 Leung and Qian 2009; Dettinger 2011). Based on the observed change in IVT, it is clear that the  
427 increase in moisture influx from past to future, which is mainly due to the change of the air water  
428 vapor content with increased temperature, corresponds to the changes of precipitation extremes  
429 shown in Figure 5.

430 1) QUANTILE CORRELATION ANALYSIS

431 To see if changes in mean precipitation can be used to predict changes in extreme precipitation  
432 features, the correlations between Pr and specific quantiles have been calculated. Here, selected  
433 quantiles including the values at 70% (70p), 80% (80p), 90% (90p), 95% (95p) and 99% (99p)  
434 are applied based on the all the daily precipitation data at each grid point within each time period.  
435 These quantiles are chosen in order to account for the changes of both moderation and extreme  
436 precipitation. The mean Pr and those quantiles for hist, and the differences of these quantities  
437 among different time periods can be found in the supplemental figure. Within expectation, regions  
438 with higher Pr are associated with larger values of those quantiles, i.e. stronger precipitation  
439 extremes. This is further supported by the high correlation (about 0.7-0.9) between Pr and R20mm,  
440 R40mm, and Rxmm, not between Pr and non-extreme precipitation events.

441 Spatial correlation is assessed by computing Pearson product-moment coefficient of linear corre-  
442 lation between relevant variables. It is found that the absolute changes of Pr in future are positively  
443 related with the absolute changes of the quantiles. This relationship is at a moderate level between  
444 mid and hist (larger than 0.65), and becomes stronger when going to the end period (reaching  
445 ~0.96). Consistently, the mean Pr itself is also positively correlated with the absolute changes of  
446 the quantiles in future (around 0.5 to 0.78), except 70p between end and mid and 99p mid and  
447 hist.

448 The relative changes of quantiles are also related with the relative changes of Pr with correla-  
449 tions around 0.65 to 0.85, except 70p and 80p between end and mid. So, the area featured with  
450 higher increase of extreme precipitations in future also tends to have larger increase of its mean  
451 precipitation. However, the wetter area does not necessary have more intense changes of moder-  
452 ate and extreme precipitation than drier area. **The changes of Pr is not obviously correlated with**  
453 **the changes of precipitation indices, which further states that mean precipitation and precipitation**  
454 **events undergo different features of changing in the future.**

455 For further investigation of the regional heterogeneity, the frequency distributions of daily rainy  
456 days for specific four regions are depicted based on simulation outputs at each gridpoint over  
457 26 years of each time period (see Figure 8). We can see over the northwest, Pr intensifies with  
458 upper tail going more extreme in the future, especially during end. No notable difference can be  
459 observed for California area, except with more extreme upper tail for Pr exceeding 100 mm/day  
460 during end, which is due to the increased precipitation extremes over the northern California as  
461 shown in Figure 6. Over the inter-mountainous region, similar trends of changes can be seen  
462 as the northwest area, with intensified mean and extreme precipitation. For the southwest area,  
463 precipitation tends to be more extreme with a moderate level, although no notable difference exists  
464 between mid and end.

## 465 2) ISOLATING DIFFERENCES DUE TO CLIMATE CHANGE AND ENSO

466 The phase of ENSO is well known to have important repercussions on precipitation extremes  
467 (Larkin and Harrison 2005; Allan and Soden 2008; Maloney et al. 2014; Yoon et al. 2015). Cai  
468 et al. (2014) found a significantly increase for extraordinary precipitation along the eastern Pacific  
469 Ocean in the 21st century within the CMIP5 ensemble, associated with increasing frequency of

extreme El Niño events due to greenhouse warming. In this part, we will figure out how the ENSO impacts specific regions over our study area, and whether the effects pattern will change over time. ENSO from past to future, the difference of precipitation behaviors between the warm phase (i.e. El Niño) and cool phase (i.e. La Niña) of ENSO is illustrated in Figure 9 for the wet seasons of each time period. Based on the ONI index values, the mean SST anomalies are 1.38, 1.71 and 2.30 K during El Niño years, and -1.16, -1.62 and -1.43 K during La Niña years for hist, mid and end respectively. The mean SSTs over the Niño 3.4 region where the are 26.83, 28.62 and 30.54°C for textsfhist, mid and end respectively. Based on the SST datasets we used here, the anomaly of ENSO has intensified. The SST anomalies of each year and each month, and their associated spatial pattern when averaged during the warm and cool phases can be found in the supplement, exhibiting the increasing frequency of El Niño during for mid and almost doubled frequency of La Niña during mid and end compared to the hist.

(Huang: As SSTs increase in the future, is not it normal for the anomaly of ENSO to be increased to compensate the changes of water vapor capacity? Might email Neale about this.)

During the El Niño phase, intensified mean precipitation is expected over the southwest (Hamlet and Lettenmaier 2007), along with reduced precipitation intensity over the northwest. In La Niña phase, the pattern is essentially reversed, with wetter conditions in the northwest and a drier situation in the Southwest. This feature is characterized as a northwest/southwest precipitation dipole, triggered by ENSO's modification of the storm track (Gershunov and Barnett 1998; Leung et al. 2003b), along with modulation of the enhanced precipitation variability (Cayan et al. 1999; Kahya and Dracup 1994). This dipole is also apparently in the frequency of rainy days and extreme precipitation events.

In mid and hist, ENSO is observed to intensify, which appears to be related with the changes of the strength of El Niño and La Niña. This can be explained by the SST anomaly magnitude

494 (detrended) of warm and cold phases (see the supplement). DeFlorio et al. (2013) also found a  
495 statistically significant linkages with ENSO and PDO for both the overall and extreme intensity  
496 of wintertime precipitation over the WUS using CCSM4 (earlier form of CESM). Strengthening  
497 storm patterns associated with ENSO are also found by Maloney et al. (2014) over California using  
498 CMIP5 output under RCP8.5.

499 We have also checked the teleconnection effect of Pacific Decadal Oscillation (PDO) and it  
500 did not show strong effect alone. Precipitation features did not change notably when at the cool  
501 phase or warm phase of PDO during hist. However, together with ENSO at the same phase,  
502 PDO can have notable effect over northwest. This coupled effect has been found by previous  
503 studies Gershunov and Barnett (1998), stating ENSO and PDO can "reinforce" each other with  
504 PDO responding to the same internal atmospheric variability as ENSO (Pierce 2002). In our  
505 simulations, the patterns of PDO phases differs quite a bit from past to future, though there were  
506 roughly an equal number of positive PDO years and negative PDO years in the data. We suppose  
507 that our 26 years simulation time period might not be long enough to account for the variability of  
508 PDO due to its duration for decades. Therefore, in this study, the PDO is not specifically analyzed.

509 The impact of ENSO is further observed by the IVT difference over rainy days between El Niño  
510 and La Niña (see Figure 10) accompanying by the wind pattern difference at 850 hPa, showing the  
511 increase of the moisture flux for the southwest and decrease for the northwest. This suggests the  
512 major role of moisture influx regulation of ENSO.

513 Based on the above results, it can be seen that the magnitude of the effects of ENSO is compara-  
514 ble or even higher than the impacts of climate forcing. For further investigation, linear regression  
515 is applied to signaling the factor effects due to ENSO and climate forcing. First, we get the SST  
516 anomaly of each cool season when ENSO mainly affect followed by the way of Niño 3.4 to be  
517 the ENSO factor values. Then, we use the GHGs values at each year to represent the climate

518 forcing factor. The features of the precipitation indices as we defined above are used as response  
519 variables. Combined the values of all the time period and all the runs, we got the significance of  
520 these two factors' effects at each grid point based on the ANOVA (analysis of variance) output  
521 (see the supplement). Changing of the SSTs anomaly can affect most of the study area for non-  
522 extreme precipitation events, and southern regions and the Cascades and the Rocky Mountains for  
523 precipitation extremes. The GHGs factor mainly shows significant impacts over the northwest and  
524 inter-mountainous regions for both non-extreme and extreme precipitation events.

525 We have also examined the linear coefficients of these two factors over where their effects are  
526 significant to see the strength that ENSO and GHGs play at each grid point (see the supplement). It  
527 is found that the effect of the ENSO is similar to the pattern of the difference between El Niño and  
528 La Niña (see Figure 10). In contrast, the effect of the GHGs is close to the pattern of the difference  
529 between the different time periods (see Figure 5). We do acknowledge that the values might not be  
530 accurate due to the simple linear mode we used here. However, the qualitative conclusions won't  
531 change. Therefore, we assume that even the ENSO largely regulates the precipitation over different  
532 phases, it won't affect our results shown here for the changes of precipitation features from past to  
533 future. Although here is just one of the possible cases of ENSO scenarios in the future, as ENSO  
534 behavior is strongly dependent on choice of climate models, the underlying principles should still  
535 be consistent.

536 Although, the strength of ENSO intensifies in the future with CESM, there is still substantial  
537 uncertainty regarding how El Niño will change under global warming as debated by plenty of  
538 studies (Fedorov and Philander 2000; Guilyardi et al. 2009), particularly as ENSO appears to be  
539 relatively insensitive to a doubling of CO<sub>2</sub> in most models (DiNezio et al. 2012). Correctly simula-  
540 tion changes to the spatial pattern of SSTs ion state-of-the-art coupled GCMs remains challenging  
541 Joseph and Nigam (2006); ?); Jha et al. (2014); Taschetto et al. (2014).

542 **7. Discussion and Summary**

543 The increased cool season precipitation extremes tend to result in higher runoff events over  
544 the northwest U.S., which are in turn associated with a greater chance of flooding and a loss of  
545 snowpack. A decrease in counts of rainy days during the warm season over central and southern  
546 California, though small in magnitude, will probably intensify the drought condition due to the  
547 deficit of soil moisture with higher evapotranspiration caused by the warmer climate in the future  
548 Cayan et al. (2010); Bell et al. (2004).

549 (Huang: Yoon et al. (2015) found a strengthened relation with ENSO for the projected increase  
550 in water cycle extremes in California using the output from CESM1 and CMIP5. Similarly by  
551 Maloney et al. (2014) using CMIP5 dataset. (check the CESM1?))

552 (Summary is to be added once the main content have been settled down The contribution of  
553 human-induced increases in greenhouse gases to the character of precipitation is confounded by  
554 patterns of variability in the atmospheric circulation. Consistent with previous studies, changes  
555 in more extreme precipitation follow the Clausius-Clapeyron relationship more closely than total  
556 precipitation amount. The changes of the strength of ENSO remains uncertain. However, the char-  
557 acter of ENSO appears to be the largest factor in understanding changing precipitation extremes  
558 in the U.S. West.)

559 *Acknowledgments.* The authors would like to thank Michael Wehner for sharing the dataset and  
560 many suggestions. The authors also want to thank Alan M. Rhoades for providing the simulation  
561 output. We acknowledge the substantial efforts behind the datasets used in this study, including  
562 UW, NCDC and NARR. The simulation data used is available by request at xyhuang@ucdavis.edu.  
563 This project is supported in part by the xxx and by the xxx.

564    **References**

- 565    AchutaRao, K., and K. R. Sperber, 2006: Enso simulation in coupled ocean-atmosphere models:  
566        are the current models better? *Climate Dynamics*, **27** (1), 1–15.
- 567    Allan, R. P., and B. J. Soden, 2008: Atmospheric warming and the amplification of precipitation  
568        extremes. *Science*, **321** (5895), 1481–1484.
- 569    Allen, M. R., and W. J. Ingram, 2002: Constraints on future changes in climate and the hydrologic  
570        cycle. *Nature*, **419** (6903), 224–232.
- 571    Bell, J. L., L. C. Sloan, and M. A. Snyder, 2004: Regional changes in extreme climatic events: a  
572        future climate scenario. *Journal of Climate*, **17** (1), 81–87.
- 573    Cai, W., and Coauthors, 2014: Increasing frequency of extreme el niño events due to greenhouse  
574        warming. *Nature climate change*, **4** (2), 111–116.
- 575    Caldwell, P., 2010: California wintertime precipitation bias in regional and global climate models.  
576        *Journal of Applied Meteorology and Climatology*, **49** (10), 2147–2158.
- 577    Capotondi, A., 2013: Enso diversity in the ncar ccm4 climate model. *Journal of Geophysical  
578        Research: Oceans*, **118** (10), 4755–4770.
- 579    Cayan, D. R., T. Das, D. W. Pierce, T. P. Barnett, M. Tyree, and A. Gershunov, 2010: Future  
580        dryness in the southwest us and the hydrology of the early 21st century drought. *Proceedings of  
581        the National Academy of Sciences*, **107** (50), 21 271–21 276.
- 582    Cayan, D. R., K. T. Redmond, and L. G. Riddle, 1999: ENSO and hydrologic extremes in the  
583        western United States\*. *Journal of Climate*, **12** (9), 2881–2893.

- 584 DeFlorio, M. J., D. W. Pierce, D. R. Cayan, and A. J. Miller, 2013: Western us extreme precipita-  
585 tion events and their relation to enso and pdo in csm4. *Journal of Climate*, **26** (12), 4231–4243.
- 586 Dennis, J., and Coauthors, 2011: CAM-SE: A scalable spectral element dynamical core for the  
587 Community Atmosphere Model. *International Journal of High Performance Computing Appli-*  
588 *cations*, 1094342011428142.
- 589 Deser, C., R. Knutti, S. Solomon, and A. S. Phillips, 2012a: Communication of the role of natural  
590 variability in future north american climate. *Nature Climate Change*, **2** (11), 775–779.
- 591 Deser, C., A. Phillips, V. Bourdette, and H. Teng, 2012b: Uncertainty in climate change projec-  
592 tions: the role of internal variability. *Climate Dynamics*, **38** (3-4), 527–546.
- 593 Deser, C., and Coauthors, 2012c: Enso and pacific decadal variability in the community climate  
594 system model version 4. *Journal of Climate*, **25** (8), 2622–2651.
- 595 Dettinger, M., 2011: Climate change, atmospheric rivers, and floods in california—a multimodel  
596 analysis of storm frequency and magnitude changes1. Wiley Online Library.
- 597 Diffenbaugh, N. S., J. S. Pal, R. J. Trapp, and F. Giorgi, 2005: Fine-scale processes regulate the  
598 response of extreme events to global climate change. *Proceedings of the National Academy of*  
599 *Sciences of the United States of America*, **102** (44), 15 774–15 778.
- 600 DiNezio, P. N., B. P. Kirtman, A. C. Clement, S.-K. Lee, G. A. Vecchi, and A. Wittenberg, 2012:  
601 Mean climate controls on the simulated response of enso to increasing greenhouse gases. *Jour-*  
602 *nal of Climate*, **25** (21), 7399–7420.
- 603 Dominguez, F., E. Rivera, D. Lettenmaier, and C. Castro, 2012: Changes in winter precipitation  
604 extremes for the western united states under a warmer climate as simulated by regional climate  
605 models. *Geophysical Research Letters*, **39** (5).

- 606 Donat, M. G., A. L. Lowry, L. V. Alexander, P. A. OGorman, and N. Maher, 2016: More extreme  
607 precipitation in the world [rsquor] s dry and wet regions. *Nature Climate Change*.
- 608 Duffy, P., and Coauthors, 2006: Simulations of present and future climates in the western United  
609 States with four nested regional climate models. *Journal of Climate*, **19** (6), 873–895.
- 610 Duli re, V., Y. Zhang, and E. P. Salath  Jr, 2011: Extreme Precipitation and Temperature over the  
611 US Pacific Northwest: A Comparison between Observations, Reanalysis Data, and Regional  
612 Models\*. *Journal of Climate*, **24** (7), 1950–1964.
- 613 Easterling, D. R., G. A. Meehl, C. Parmesan, S. A. Changnon, T. R. Karl, and L. O. Mearns, 2000:  
614 Climate extremes: observations, modeling, and impacts. *science*, **289** (5487), 2068–2074.
- 615 Fedorov, A. V., and S. G. Philander, 2000: Is el ni o changing? *Science*, **288** (5473), 1997–2002.
- 616 Fox-Rabinovitz, M., J. C te, B. Dugas, M. D qu , and J. L. McGregor, 2006: Variable resolution  
617 general circulation models: Stretched-grid model intercomparison project (SGMIP). *Journal of  
618 Geophysical Research: Atmospheres (1984–2012)*, **111** (D16).
- 619 Fox-Rabinovitz, M. S., G. L. Stenchikov, M. J. Suarez, and L. L. Takacs, 1997: A finite-  
620 difference GCM dynamical core with a variable-resolution stretched grid. *Monthly weather  
621 review*, **125** (11), 2943–2968.
- 622 Frei, C., R. Sch ll, S. Fukutome, J. Schmidli, and P. L. Vidale, 2006: Future change of precipita-  
623 tion extremes in Europe: Intercomparison of scenarios from regional climate models. *Journal  
624 of Geophysical Research: Atmospheres (1984–2012)*, **111** (D6).
- 625 Gao, Y., J. Lu, L. R. Leung, Q. Yang, S. Hagos, and Y. Qian, 2015: Dynamical and thermodynamical  
626 modulations on future changes of landfalling atmospheric rivers over western north america.  
627 *Geophysical Research Letters*, **42** (17), 7179–7186.

- 628 Gates, W. L., 1992: AMIP: The Atmospheric Model Intercomparison Project. *Bulletin of the*  
629 *American Meteorological Society*, **73**, 1962–1970.
- 630 Gershunov, A., and T. P. Barnett, 1998: Interdecadal modulation of enso teleconnections. *Bulletin*  
631 *of the American Meteorological Society*, **79 (12)**, 2715–2725.
- 632 Grodsky, S. A., J. A. Carton, S. Nigam, and Y. M. Okumura, 2012: Tropical atlantic biases in  
633 ccsm4. *Journal of Climate*, **25 (11)**, 3684–3701.
- 634 Guilyardi, E., A. Wittenberg, A. Fedorov, M. Collins, C. Wang, A. Capotondi, G. J. Van Olden-  
635 borgh, and T. Stockdale, 2009: Understanding el niño in ocean-atmosphere general circulation  
636 models. *Bulletin of the American Meteorological Society*, **90 (3)**, 325.
- 637 Hamlet, A. F., and D. P. Lettenmaier, 2005: Production of Temporally Consistent Gridded Precipi-  
638 tation and Temperature Fields for the Continental United States\*. *Journal of Hydrometeorology*,  
639 **6 (3)**, 330–336.
- 640 Hamlet, A. F., and D. P. Lettenmaier, 2007: Effects of 20th century warming and climate variability  
641 on flood risk in the western us. *Water Resources Research*, **43 (6)**.
- 642 Hegerl, G. C., F. W. Zwiers, P. A. Stott, and V. V. Kharin, 2004: Detectability of anthropogenic  
643 changes in annual temperature and precipitation extremes. *Journal of Climate*, **17 (19)**, 3683–  
644 3700.
- 645 Huang, X., A. M. Rhoades, P. A. Ullrich, and C. M. Zarzycki, 2016: An evaluation of the vari-  
646 able resolution-cesm for modeling california’s climate. *Journal of Advances in Modeling Earth*  
647 *Systems*.
- 648 Huang, X., and P. A. Ullrich, 2016: Irrigation impacts on california’s climate with the variable-  
649 resolution cesm. *Journal of Advances in Modeling Earth Systems*.

- 650 Hurrell, J. W., J. J. Hack, D. Shea, J. M. Caron, and J. Rosinski, 2008: A new sea surface temper-  
651 ature and sea ice boundary dataset for the Community Atmosphere Model. *Journal of Climate*,  
652 **21 (19)**, 5145–5153.
- 653 Hurrell, J. W., and Coauthors, 2013: The community earth system model: A framework for col-  
654 laborative research. *Bulletin of the American Meteorological Society*, **94 (9)**, 1339–1360.
- 655 Jha, B., Z.-Z. Hu, and A. Kumar, 2014: Sst and enso variability and change simulated in historical  
656 experiments of cmip5 models. *Climate dynamics*, **42 (7-8)**, 2113–2124.
- 657 Joseph, R., and S. Nigam, 2006: Enso evolution and teleconnections in ipcc’s twentieth-century  
658 climate simulations: Realistic representation? *Journal of Climate*, **19 (17)**, 4360–4377.
- 659 Joshi, M. M., J. M. Gregory, M. J. Webb, D. M. Sexton, and T. C. Johns, 2008: Mechanisms for  
660 the land/sea warming contrast exhibited by simulations of climate change. *Climate Dynamics*,  
661 **30 (5)**, 455–465.
- 662 Kahya, E., and J. A. Dracup, 1994: The influences of type 1 el nino and la nina events on stream-  
663 flows in the pacific southwest of the united states. *Journal of Climate*, **7 (6)**, 965–976.
- 664 Kao, H.-Y., and J.-Y. Yu, 2009: Contrasting eastern-pacific and central-pacific types of enso.  
665 *Journal of Climate*, **22 (3)**, 615–632.
- 666 Karl, T. R., N. Nicholls, and A. Ghazi, 1999: Clivar/gcos/wmo workshop on indices and indicators  
667 for climate extremes workshop summary. *Weather and Climate Extremes*, Springer, 3–7.
- 668 Kharin, V. V., F. W. Zwiers, X. Zhang, and G. C. Hegerl, 2007: Changes in temperature and  
669 precipitation extremes in the IPCC ensemble of global coupled model simulations. *Journal of*  
670 *Climate*, **20 (8)**, 1419–1444.

- 671 Kim, J., 2005: A projection of the effects of the climate change induced by increased co2 on  
672 extreme hydrologic events in the western us. *Climatic Change*, **68** (1-2), 153–168.
- 673 Laprise, R., and Coauthors, 2008: Challenging some tenets of regional climate modelling. *Meteo-*  
674 *rology and Atmospheric Physics*, **100** (1-4), 3–22.
- 675 Larkin, N. K., and D. Harrison, 2005: On the definition of el niño and associated seasonal average  
676 us weather anomalies. *Geophysical Research Letters*, **32** (13).
- 677 Leung, L. R., L. O. Mearns, F. Giorgi, and R. L. Wilby, 2003a: Regional climate research: needs  
678 and opportunities. *Bulletin of the American Meteorological Society*, **84** (1), 89–95.
- 679 Leung, L. R., and Y. Qian, 2009: Atmospheric rivers induced heavy precipitation and flooding in  
680 the western US simulated by the WRF regional climate model. *Geophysical research letters*,  
681 **36** (3).
- 682 Leung, L. R., Y. Qian, and X. Bian, 2003b: Hydroclimate of the western United States based on  
683 observations and regional climate simulation of 1981-2000. Part I: Seasonal statistics. *Journal*  
684 *of Climate*, **16** (12), 1892–1911.
- 685 Maloney, E. D., and Coauthors, 2014: North american climate in cmip5 experiments: part iii:  
686 assessment of twenty-first-century projections\*. *Journal of Climate*, **27** (6), 2230–2270.
- 687 Maurer, E., A. Wood, J. Adam, D. Lettenmaier, and B. Nijssen, 2002: A long-term hydrologically  
688 based dataset of land surface fluxes and states for the conterminous United States\*. *Journal of*  
689 *climate*, **15** (22), 3237–3251.
- 690 McDonald, A., 2003: Transparent boundary conditions for the shallow-water equations: testing in  
691 a nested environment. *Monthly weather review*, **131** (4), 698–705.

- 692 Meehl, G. A., H. Teng, and G. Branstator, 2006: Future changes of el niño in two global coupled  
693 climate models. *Climate Dynamics*, **26** (6), 549–566.
- 694 Mesinger, F., and K. Veljovic, 2013: Limited area NWP and regional climate modeling: a test  
695 of the relaxation vs Eta lateral boundary conditions. *Meteorology and Atmospheric Physics*,  
696 **119** (1-2), 1–16.
- 697 Mesinger, F., and Coauthors, 2006: North American regional reanalysis. *Bulletin of the American  
698 Meteorological Society*, **87**, 343–360.
- 699 Min, S.-K., X. Zhang, F. W. Zwiers, and G. C. Hegerl, 2011: Human contribution to more-intense  
700 precipitation extremes. *Nature*, **470** (7334), 378–381.
- 701 Neale, R. B., and Coauthors, 2010a: Description of the NCAR community atmosphere model  
702 (CAM 5.0). *NCAR Tech. Note NCAR/TN-486+STR*.
- 703 Neale, R. B., and Coauthors, 2010b: Description of the NCAR Community Atmosphere Model  
704 (CAM 5.0). NCAR Technical Note NCAR/TN-486+STR, National Center for Atmospheric Re-  
705 search, Boulder, Colorado, 268 pp.
- 706 Neelin, J. D., B. Langenbrunner, J. E. Meyerson, A. Hall, and N. Berg, 2013: California winter  
707 precipitation change under global warming in the coupled model intercomparison project phase  
708 5 ensemble. *Journal of Climate*, **26** (17), 6238–6256.
- 709 Neiman, P. J., F. M. Ralph, G. A. Wick, J. D. Lundquist, and M. D. Dettinger, 2008: Meteorolog-  
710 ical characteristics and overland precipitation impacts of atmospheric rivers affecting the west  
711 coast of north america based on eight years of ssm/i satellite observations. *Journal of Hydrom-  
712 eteorology*, **9** (1), 22–47.

- 713 NOAA, 2013: Defining El Niño and La Niña. Accessed: 2015-
- 714 08-20, [https://www.climate.gov/news-features/understanding-climate/  
watching-el-nio-and-la-nia-noaa-adapts-global-warming](https://www.climate.gov/news-features/understanding-climate/watching-el-nio-and-la-nia-noaa-adapts-global-warming).
- 715
- 716 O’Gorman, P. A., and T. Schneider, 2009: The physical basis for increases in precipitation ex-
- 717 tremes in simulations of 21st-century climate change. *Proceedings of the National Academy of*
- 718 *Sciences*, **106 (35)**, 14 773–14 777.
- 719 Oleson, K., and Coauthors, 2010: Technical description of version 4.0 of the Community Land
- 720 Model (CLM). NCAR Technical Note NCAR/TN-478+STR, National Center for Atmospheric
- 721 Research, Boulder, Colorado, 257 pp. doi:10.5065/D6FB50WZ.
- 722 Pierce, D. W., 2002: The role of sea surface temperatures in interactions between enso and the
- 723 north pacific oscillation. *Journal of climate*, **15 (11)**, 1295–1308.
- 724 Ralph, F. M., P. J. Neiman, and G. A. Wick, 2004: Satellite and caljet aircraft observations of
- 725 atmospheric rivers over the eastern north pacific ocean during the winter of 1997/98. *Monthly*
- 726 *Weather Review*, **132 (7)**, 1721–1745.
- 727 Rauscher, S. A., E. Coppola, C. Piani, and F. Giorgi, 2010: Resolution effects on regional climate
- 728 model simulations of seasonal precipitation over Europe. *Climate dynamics*, **35 (4)**, 685–711.
- 729 Rauscher, S. A., T. D. Ringler, W. C. Skamarock, and A. A. Mirin, 2013: Exploring a Global
- 730 Multiresolution Modeling Approach Using Aquaplanet Simulations. *Journal of Climate*, **26 (8)**,
- 731 2432–2452.
- 732 Rhoades, A. M., X. Huang, P. A. Ullrich, and C. M. Zarzycki, 2015: Characterizing Sierra Nevada
- 733 snowpack using variable-resolution CESM. *Journal of Applied Meteorology and Climatology*,
- 734 **(2015)**.

- 735 Riahi, K., and Coauthors, 2011: RCP 8.5A scenario of comparatively high greenhouse gas emissions.  
736 *Climatic Change*, **109** (1-2), 33–57.
- 737 Rowell, D. P., and R. G. Jones, 2006: Causes and uncertainty of future summer drying over europe.  
738 *Climate Dynamics*, **27** (2-3), 281–299.
- 739 Salathé Jr, E. P., R. Steed, C. F. Mass, and P. H. Zahn, 2008: A High-Resolution Climate Model  
740 for the US Pacific Northwest: Mesoscale Feedbacks and Local Responses to Climate Change\*.  
741 *Journal of Climate*, **21** (21), 5708–5726.
- 742 Scoccimarro, E., M. Zampieri, A. Bellucci, A. Navarra, and Coauthors, 2013: Heavy precipitation  
743 events in a warmer climate: results from CMIP5 models. *Journal of climate*.
- 744 Seneviratne, S. I., and Coauthors, 2012: Changes in climate extremes and their impacts on the  
745 natural physical environment. *Managing the risks of extreme events and disasters to advance  
746 climate change adaptation*, 109–230.
- 747 Sillmann, J., V. Kharin, F. Zwiers, X. Zhang, and D. Bronaugh, 2013: Climate extremes indices  
748 in the cmip5 multimodel ensemble: Part 2. future climate projections. *Journal of Geophysical  
749 Research: Atmospheres*, **118** (6), 2473–2493.
- 750 Simmons, A., K. Willett, P. Jones, P. Thorne, and D. Dee, 2010: Low-frequency variations  
751 in surface atmospheric humidity, temperature, and precipitation: Inferences from reanalyses  
752 and monthly gridded observational data sets. *Journal of Geophysical Research: Atmospheres*,  
753 **115** (D1).
- 754 Singh, D., M. Tsiang, B. Rajaratnam, and N. S. Diffenbaugh, 2013: Precipitation extremes over the  
755 continental United States in a transient, high-resolution, ensemble climate model experiment.  
756 *Journal of Geophysical Research: Atmospheres*, **118** (13), 7063–7086.

- 757 Small, R. J., and Coauthors, 2014: A new synoptic scale resolving global climate simulation using  
758 the community earth system model. *Journal of Advances in Modeling Earth Systems*, **6** (4),  
759 1065–1094.
- 760 Staniforth, A. N., and H. L. Mitchell, 1978: A variable-resolution finite-element technique for  
761 regional forecasting with the primitive equations. *Monthly Weather Review*, **106** (4), 439–447.
- 762 Sugi, M., and J. Yoshimura, 2004: A mechanism of tropical precipitation change due to co2  
763 increase. *Journal of climate*, **17** (1), 238–243.
- 764 Taschetto, A. S., A. S. Gupta, N. C. Jourdain, A. Santoso, C. C. Ummenhofer, and M. H. England,  
765 2014: Cold tongue and warm pool enso events in cmip5: mean state and future projections.  
766 *Journal of Climate*, **27** (8), 2861–2885.
- 767 Taylor, M. A., 2011: Conservation of mass and energy for the moist atmospheric primitive equa-  
768 tions on unstructured grids. *Numerical Techniques for Global Atmospheric Models*, Springer,  
769 357–380.
- 770 Tebaldi, C., K. Hayhoe, J. M. Arblaster, and G. A. Meehl, 2006: Going to the extremes. *Climatic  
771 change*, **79** (3-4), 185–211.
- 772 Trenberth, K. E., 2011: Changes in precipitation with climate change. *Climate Research*, **47** (1),  
773 123.
- 774 Trenberth, K. E., A. Dai, R. M. Rasmussen, and D. B. Parsons, 2003: The changing character of  
775 precipitation. *Bulletin of the American Meteorological Society*, **84** (9), 1205–1217.
- 776 Walker, M. D., and N. S. Diffenbaugh, 2009: Evaluation of high-resolution simulations of daily-  
777 scale temperature and precipitation over the united states. *Climate dynamics*, **33** (7-8), 1131–  
778 1147.

- 779 Wehner, M. F., 2013: Very extreme seasonal precipitation in the NARCCAP ensemble: model  
780 performance and projections. *Climate Dynamics*, **40** (1-2), 59–80.
- 781 Wehner, M. F., R. L. Smith, G. Bala, and P. Duffy, 2010: The effect of horizontal resolution  
782 on simulation of very extreme US precipitation events in a global atmosphere model. *Climate  
783 dynamics*, **34** (2-3), 241–247.
- 784 Wehner, M. F., and Coauthors, 2014: The effect of horizontal resolution on simulation qual-  
785 ity in the Community Atmospheric Model, CAM5.1. *J. Model. Earth. Sys.*, doi:10.1002/  
786 2013MS000276.
- 787 Yoon, J.-H., S. S. Wang, R. R. Gillies, B. Kravitz, L. Hipps, and P. J. Rasch, 2015: Increasing  
788 water cycle extremes in California and in relation to ENSO cycle under global warming. *Nature  
789 communications*, **6**.
- 790 Zarzycki, C. M., C. Jablonowski, and M. A. Taylor, 2014: Using Variable-Resolution Meshes  
791 to Model Tropical Cyclones in the Community Atmosphere Model. *Monthly Weather Review*,  
792 **142** (3), 1221–1239.
- 793 Zarzycki, C. M., C. Jablonowski, D. R. Thatcher, and M. A. Taylor, 2015: Effects of localized grid  
794 refinement on the general circulation and climatology in the Community Atmosphere Model.  
795 *Journal of Climate*, (2015).
- 796 Zhang, X., L. Alexander, G. C. Hegerl, P. Jones, A. K. Tank, T. C. Peterson, B. Trewin, and  
797 F. W. Zwiers, 2011: Indices for monitoring changes in extremes based on daily temperature and  
798 precipitation data. *Wiley Interdisciplinary Reviews: Climate Change*, **2** (6), 851–870.

799 Zhang, X., J. Wang, F. W. Zwiers, and P. Y. Groisman, 2010: The influence of large-scale climate  
800 variability on winter maximum daily precipitation over North America. *Journal of Climate*,  
801 **23 (11)**, 2902–2915.

802 update the mesh grid plot

803 update the plot with new label levels

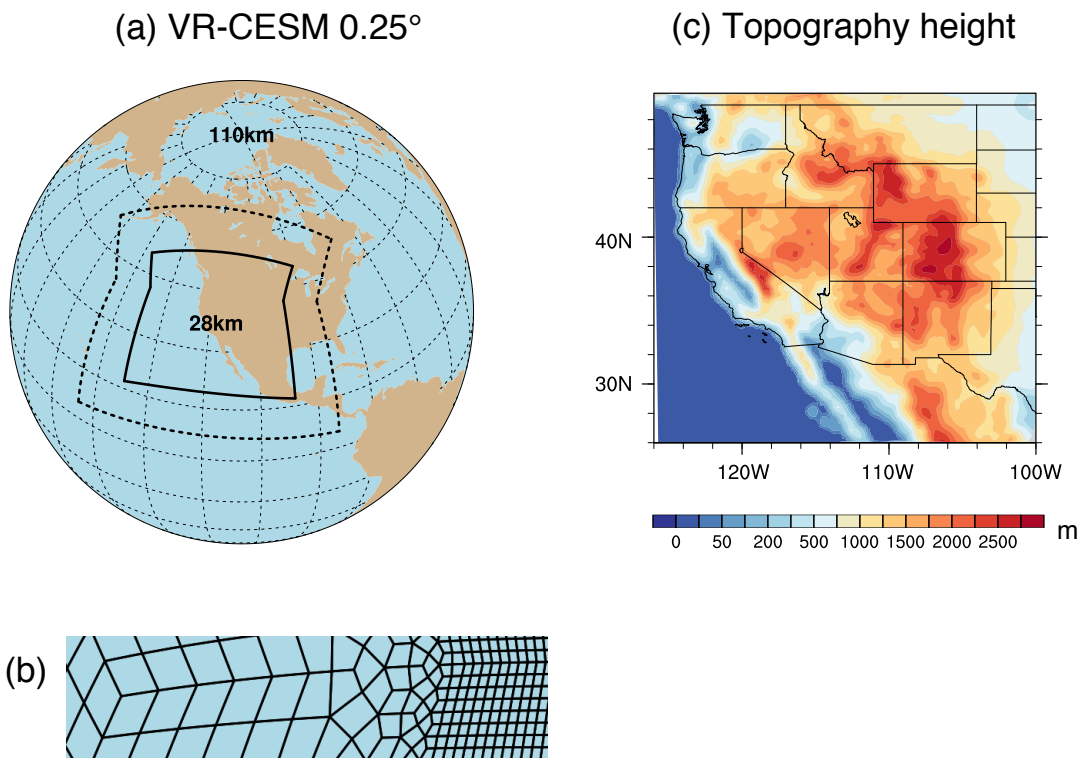
804 LIST OF TABLES

TABLE 1. Precipitation indices employed in this study.

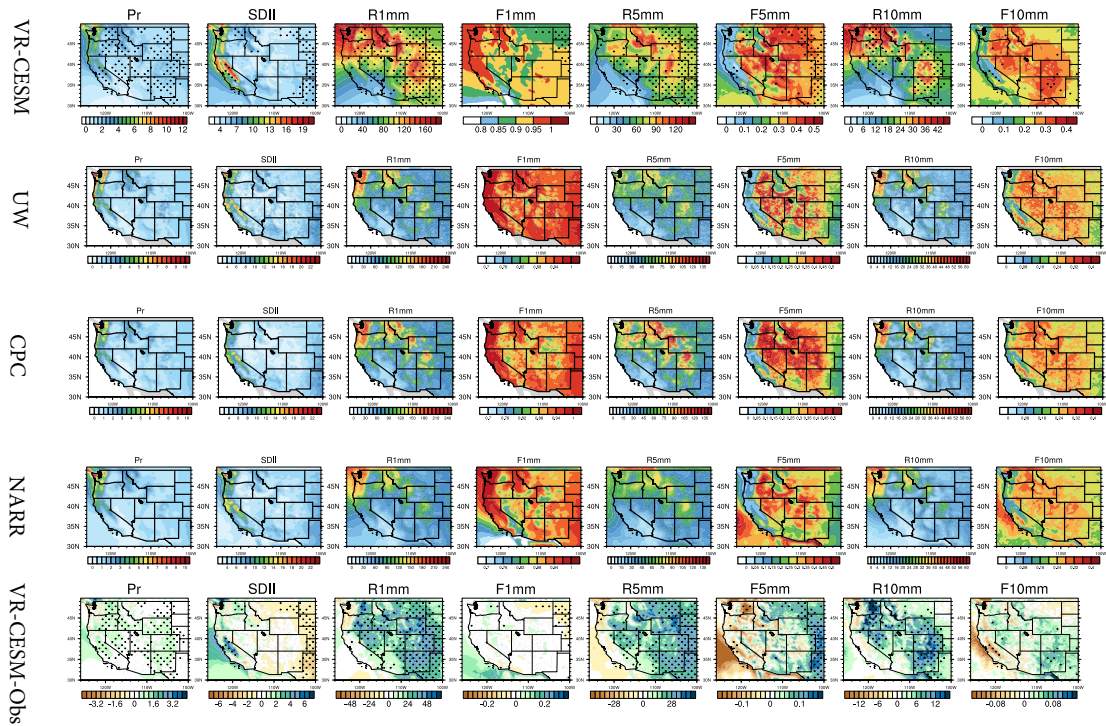
Name	Definition
Pr	Mean daily precipitation
R1mm	Number of days per year with Pr>1 mm
SDII	Simple precipitation intensity index: Precipitation amount / $\langle R1mm \rangle$ (mm/day)
R5mm	Number of days per year with Pr>1 mm and Pr=<5 mm
R10mm	Number of days per year with Pr>5 mm and Pr=<10 mm
R20mm	Number of days per year with Pr>10 mm and Pr=<20 mm
R40mm	Number of days per year with Pr>20 mm and Pr=<40 mm
Rxmm	Number of days per year with Pr>40 mm
F1mm	Fraction of precipitation contributed to the total precipitation for days of R1mm (similarly for F5mm, F10mm, F20mm, F40mm and Fxmm)
P5mm	Precipitation amount from R5mm (similarly for P10mm, P20mm, F40mm, Pxmm)

## 806 LIST OF FIGURES

807	<b>Fig. 1.</b> (a) The approximate grid spacing used for the VR-CESM $0.25^{\circ}$ mesh. (b) A depiction of 808 the transition from the global $1^{\circ}$ resolution mesh through two layers of refinement to $0.25^{\circ}$ . 809 (c) Topography height over the study area. . . . .	42
810	<b>Fig. 2.</b> Mean precipitation and other related indices from VR-CESM and reference datasets over 811 1980-2005. (Note: Grids with statistically significance difference are marked with stip- 812 pling.) . . . . .	43
813	<b>Fig. 3.</b> The mean precipitation and other related indices from VR-CESM and reference datasets 814 over 1980-2005 (continued). . . . .	44
815	<b>Fig. 4.</b> The mean precipitation ( $Pr$ ), 2m average temperature ( $T2avg$ ), and 2m relative humidity 816 ( $RH$ ) averaged over each time period. (Note: Grids with statistically significance difference 817 for the $RH$ are marked with stippling.) . . . . .	45
818	<b>Fig. 5.</b> Differences of precipitation behaviors from past to future over WUS averaged of each time 819 period. (Note: Grids with statistically significance difference are marked with stippling.) . . . . .	46
820	<b>Fig. 6.</b> Differences of precipitation behaviors from past to future over WUS averaged of each time 821 period (continued). . . . .	47
822	<b>Fig. 7.</b> Changes of specific humidity and horizontal wind pattern at 850hPa for moisture flux il- 823 lustration, and IVT for simulations under different time period of wet season (October to 824 March). (Note: The minimum wind vector is set to be 0.5 m/s, therefore, the wind less than 825 0.5 m/s is also plotted at the minimum length for better visualization.) <b>For all difference</b> 826 <b>plots, make sure to use a common [min,max] range as its currently difficult to tease out dif-</b> 827 <b>ferences. Difference plots should also use a different color table to the mean results (perhaps</b> 828 <b>a single color color table?).</b> . . . . .	48
829	<b>Fig. 8.</b> Frequency distribution of rainy days ( $Pr >= 0.1\text{mm/day}$ ) over the three time periods from 830 simulations in four regions (with logarithmic vertical scale). (Note: Region 1 to 4 cover 831 Washington and Oregon; California; Nevada, Utah and Idaho; Arizona and New Mexico, 832 respectively.) . . . . .	49
833	<b>Fig. 9.</b> Difference of precipitation behaviors between warm and cool phases of ENSO from past to 834 future over WUS averaged of each time period. . . . .	50
835	<b>Fig. 10.</b> Changes of IVT for simulations under different phases of ENSO of wet season (October to 836 March). (Note: The minimum wind vector is set to be 0.5 m/s, therefore, the wind less than 837 0.5 m/s is also plotted at the minimum length for better visualization.) . . . . .	51

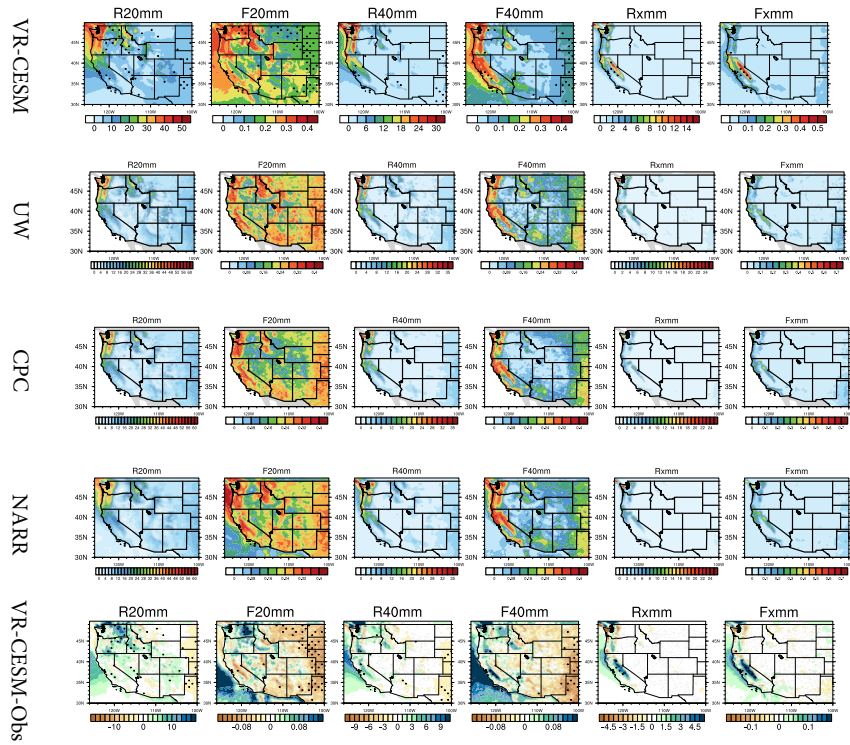


838 FIG. 1. (a) The approximate grid spacing used for the VR-CESM  $0.25^\circ$  mesh. (b) A depiction of the transition  
 839 from the global  $1^\circ$  resolution mesh through two layers of refinement to  $0.25^\circ$ . (c) Topography height over the  
 840 study area.

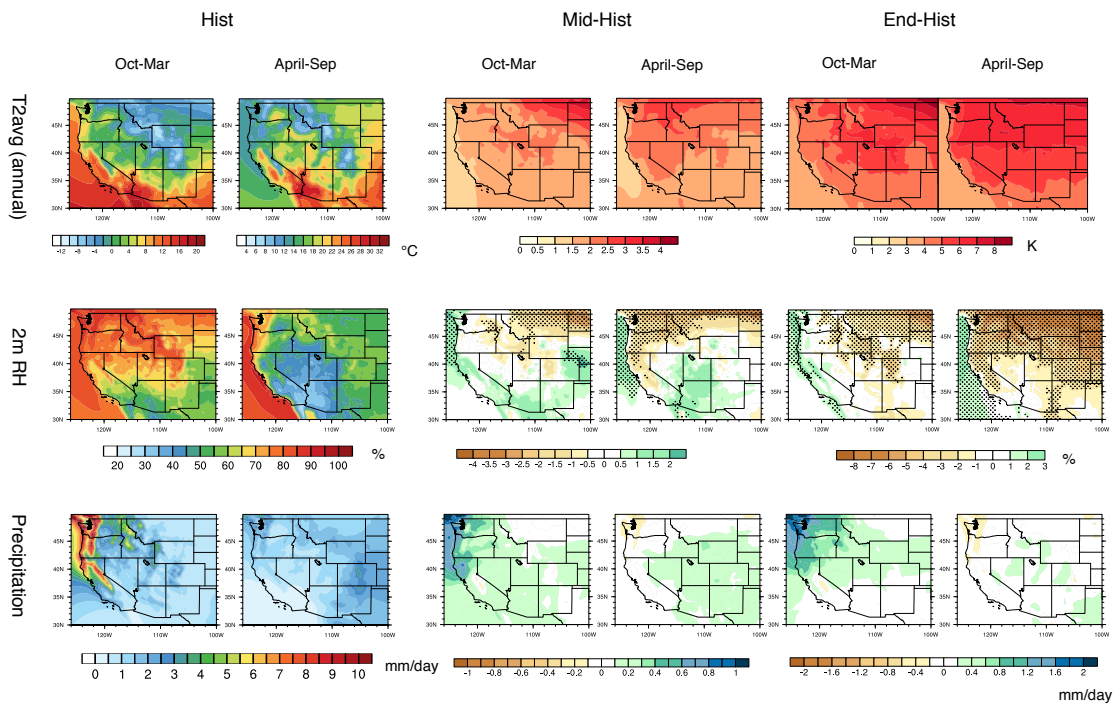


841 FIG. 2. Mean precipitation and other related indices from VR-CESM and reference datasets over 1980-2005.

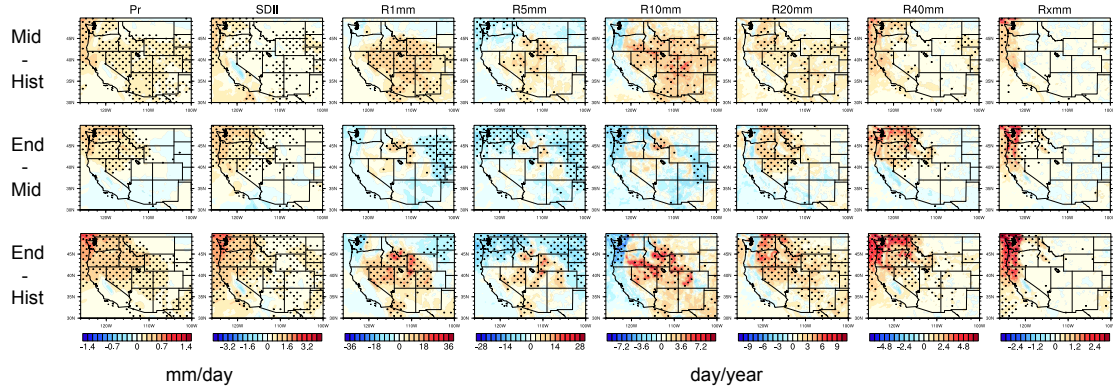
842 (Note: Grids with statistically significant difference are marked with stippling.)



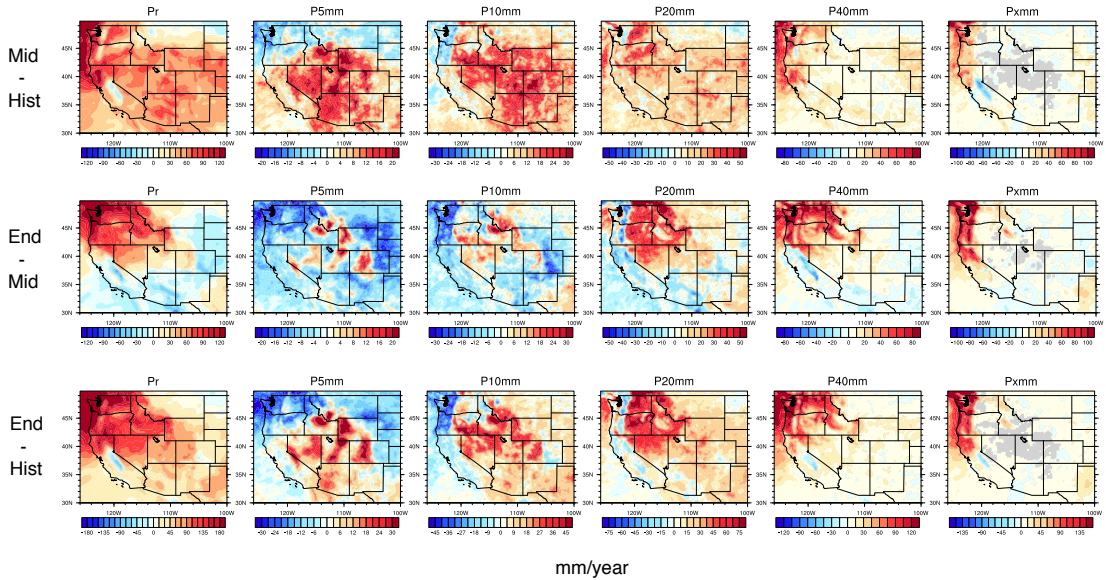
843 FIG. 3. The mean precipitation and other related indices from VR-CESM and reference datasets over 1980-  
844 2005 (continued).



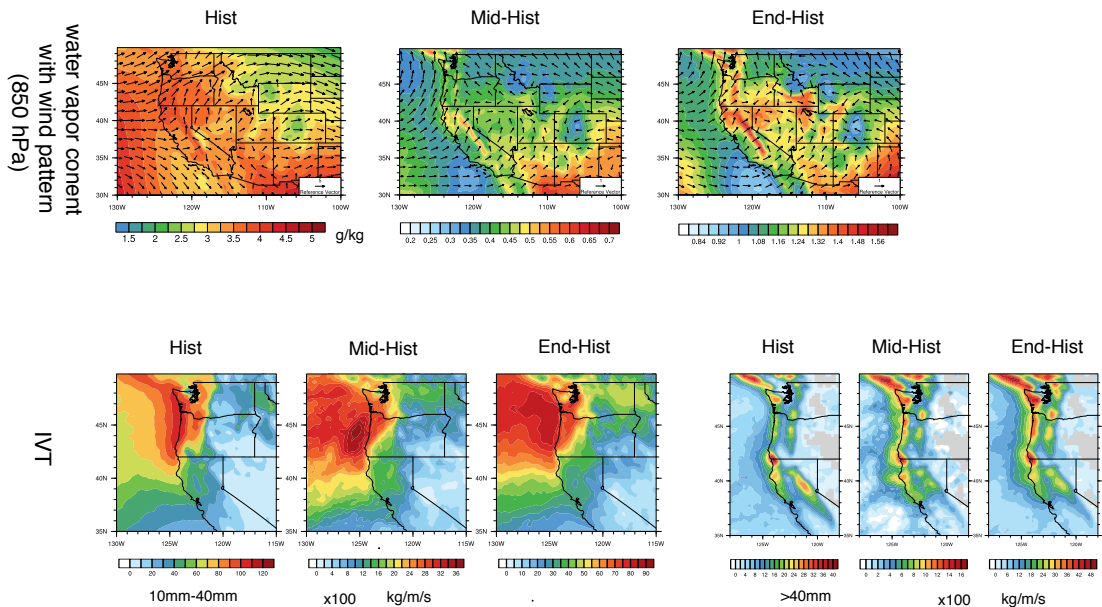
845 FIG. 4. The mean precipitation (Pr), 2m average temperature (T2avg), and 2m relative humidity (RH) aver-  
 846 aged over each time period. (Note: Grids with statistically significant difference for the RH are marked with  
 847 stippling.)



848 FIG. 5. Differences of precipitation behaviors from past to future over WUS averaged of each time period.  
 849 (Note: Grids with statistically significance difference are marked with stippling.)



850 FIG. 6. Differences of precipitation behaviors from past to future over WUS averaged of each time period  
 851 (continued).



852 FIG. 7. Changes of specific humidity and horizontal wind pattern at 850hPa for moisture flux illustration, and  
 853 IVT for simulations under different time period of wet season (October to March). (Note: The minimum wind  
 854 vector is set to be 0.5 m/s, therefore, the wind less than 0.5 m/s is also plotted at the minimum length for better  
 855 visualization.) For all difference plots, make sure to use a common [min,max] range as its currently difficult  
 856 to tease out differences. Difference plots should also use a different color table to the mean results (perhaps a  
 857 single color color table?).

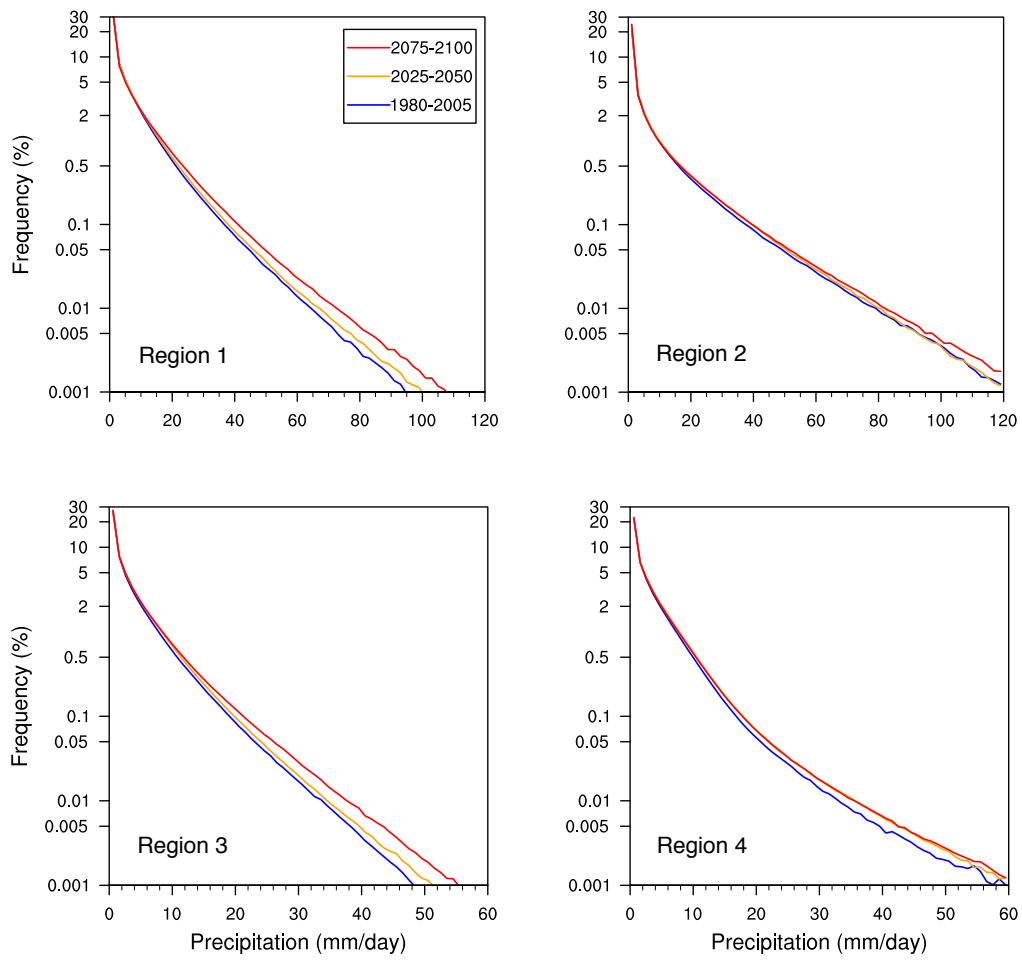
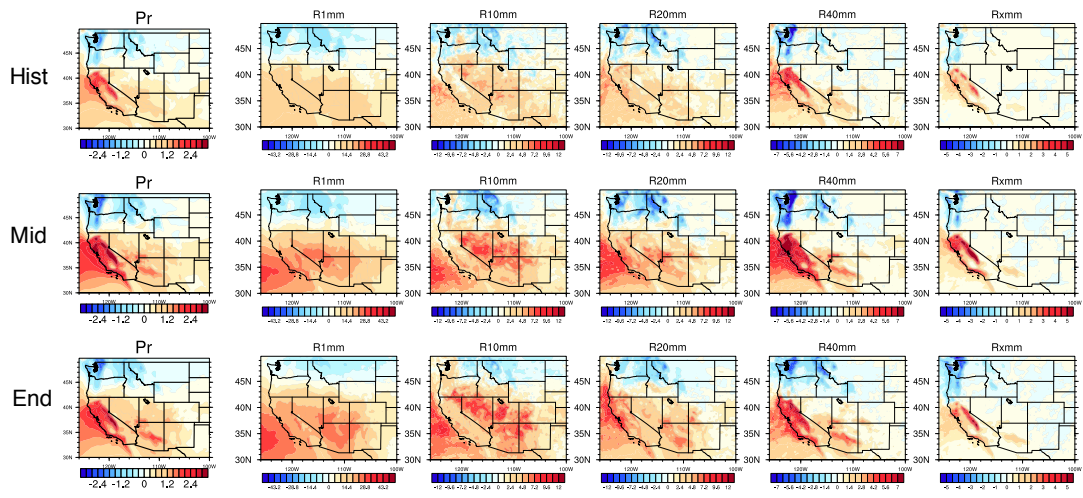
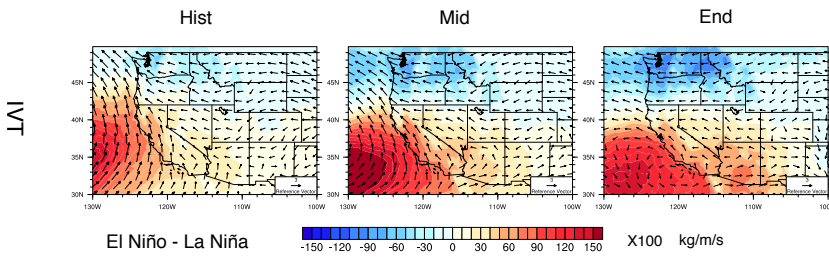


FIG. 8. Frequency distribution of rainy days ( $Pr \geq 0.1 \text{ mm/day}$ ) over the three time periods from simulations in four regions (with logarithmic vertical scale). (Note: Region 1 to 4 cover Washington and Oregon; California; Nevada, Utah and Idaho; Arizona and New Mexico, respectively.)



861 FIG. 9. Difference of precipitation behaviors between warm and cool phases of ENSO from past to future  
 862 over WUS averaged of each time period.



863 FIG. 10. Changes of IVT for simulations under different phases of ENSO of wet season (October to March).  
 864 (Note: The minimum wind vector is set to be 0.5 m/s, therefore, the wind less than 0.5 m/s is also plotted at the  
 865 minimum length for better visualization.)